Expansion of *in vitro Toxoplasma gondii* cysts using enzymatically enhanced ultrastructure expansion microscopy

Kseniia Bondarenko[1], Floriane Limoge[2], Kayvon Pedram[3], Mathieu Gissot[2], Joanna C. Young[1]

Authors

[1]Institute of Immunology and Infection Research, School of Biological Sciences, Ashworth laboratories, University of Edinburgh, Edinburgh EH9 3FL, United Kingdom

[2]U1019-UMR 9017-CIIL-Center for Infection and Immunity of Lille, University of Lille, CNRS, Inserm, CHU Lille, Institut Pasteur de Lille, F-59000 Lille, France

[3]Janelia Research Campus, Howard Hughes Medical Institute, Ashburn, VA, USA

Abstract

Expansion microscopy (ExM) is an innovative approach to achieve super-resolution images without using super-resolution microscopes, based on the physical expansion of the sample. The advent of ExM has unlocked super-resolution imaging for a broader scientific circle, lowering the cost and entry skill requirements to the field. One of its branches, ultrastructure ExM (U-ExM), has become popular among research groups studying Apicomplexan parasites, including the acute stage of *Toxoplasma gondii* infection. The chronic cyst-forming stage of *Toxoplasma*, however, resists U-ExM expansion, impeding precise protein localisation. Here, we solve the *in vitro* cyst's resistance to denaturation required for successful U-ExM of the encapsulated parasites. As the cyst's main structural protein CST1 contains a mucin domain, we added an enzymatic digestion step using the pan-mucinase StcE prior to the expansion protocol. This allowed full expansion of the cysts in fibroblasts and primary neuronal cell culture without interference with the epitopes of the cyst-wall associated proteins. Using StcE-enhanced U-ExM, we clarified the shape and location of the GRA2 protein important for establishing a normal cyst. Expanded cysts revealed GRA2 granules spanning across the cyst wall, with a notable presence observed outside on both sides of the CST1-positive layer.

Importance

Toxoplasma gondii is an intracellular parasite capable of establishing long-term chronic infection in nearly all warm-blooded animals. During the chronic stage, parasites encapsulate into cysts in a wide range of tissues but particularly in neurons of the central nervous system and in skeletal muscle. Current anti-Toxoplasma drugs do not eradicate chronic parasites and leave behind a reservoir of infection. As the cyst is critical for both transmission and pathology of the disease, we need to understand more fully the biology of the cyst and its vulnerabilities.

The advent of a new super-resolution approach called ultrastructure expansion microscopy allowed in-depth studies of the acute stage of *Toxoplasma* infection but not the cyst-forming stage, which resists protocol-specific denaturation. Here, we show that an additional step of enzymatic digestion using mucinase StcE allows full expansion of the *Toxoplasma* cysts, offering a new avenue for a comprehensive examination of the chronic stage of infection using an accessible super-resolution technique.

Introduction

Expansion Microscopy (ExM) is an imaging protocol that bypasses the diffraction limit of conventional light microscopes (~200 nm) by physically expanding the biological sample embedded in a gel (1). As an accessible alternative to Electron Microscopy, ExM has been transformative across diverse research fields, allowing nanoscale resolution of protein localisation using light microscopes.

Among the numerous ExM protocols developed so far, Ultrastructure Expansion Microscopy (U-ExM) (2) gained popularity in the field of parasitology due to the improved preservation of subcellular structures (3) U-ExM allows 4-4.5x expansion of the biological specimen (~90-fold increase in volume) with the preservation of the proteins, in contrast to other approaches which leave only the protein footprint after proteolytic digestion (2, 4). U-ExM therefore enables all-protein staining using non-specific protein dyes like N-hydroxysuccinimde (NHS) esters (5). U-ExM has been widely adopted in Apicomplexan research, generating new insights in to diverse parasite lifecycle stages and clarifying the localisation of over 80 proteins in *Toxoplasma gondii* (6–14) *,* Cryptosporidium parvum *(15, 16)* and *Plasmodium species* (5, 17–26)*.* However, investigations of the chronic *Toxoplasma gondii* cyst have lagged behind.

Toxoplasma is a single celled intracellular parasite capable of establishing long-term chronic infection in nearly all warm-blooded animals, including humans (27). *Toxoplasma* has a complex life cycle and differentiates between two non-sexual forms within intermediate hosts (28). During the acute stage of infection, the parasites replicate rapidly as so-called tachyzoites and disseminate around the host's body. To establish long-term infection, parasites differentiate to slow growing bradyzoites and develop cysts predominantly in the central nervous system and skeletal muscle. Reactivation of latent cysts can cause fatal encephalitis in the immunocompromised or recurrent ocular disease (retinochoroiditis)(29).

Toxoplasma tissue cysts are intracellular and are spherical structures 5-100 um in diameter (28), containing a collection of tightly packed bradyzoites. The cyst wall is between 250 and 850 nm thick and composed of a granular layer of proteins and carbohydrates underneath the limiting membrane (a modified version of the parasitophorous vacuole (PV) membrane which forms as the parasite invades the host cell). The accumulation of glycoproteins in the cyst wall ensures structural and chemical rigidity (30), and is thought to allow parasite transmission to infect a new host following ingestion of undercooked meat.

Toxoplasma cysts can also be generated *in vitro* in tissue culture, which has proved a valuable model for studying cyst biology. *Toxoplasma* tachyzoites differentiate to bradyzoites under stress conditions with alkaline stress the most commonly used method (31, 32). However, recent advances have improved the model with spontaneous differentiation to bradyzoites in myotubes and neurons, producing longer lasting cysts (14-28 days) (33, 34).

The cyst wall contains markers exclusively expressed during the chronic stage (35). One of the early chronic-stage markers, CST1, is major structural element of the cyst wall and parasites lacking *cst1* form fragile cysts (30). CST1 has a highly O-glycosylated mucin domain which binds to the lectin Dolichos Biflorus agglutinin (DBA) (30, 36). The structure of CST1's mucin domain includes 20 threonine-rich tandem repeats, which undergo O-GalNAc glycosylation. This glycosylation process is initiated by a group of enzymes known as polypeptide N-acetylgalactosaminyltransferases (ppGalNAc-Ts, (30, 36)). Previous studies using electron microscopy have shown that CST1 is expressed in the granular material in the cyst wall under the limiting membrane (37). It's been

hypothesised that the high glycosylation of the CST1 mucin domain could act as a bonding agent for other proteins associated with the cyst wall, such as dense granule proteins (GRAs) (38).

Toxoplasma GRAs are secreted from dense granules into the PV lumen or out into the host cell and perform a variety of functions during infection including mediating host–parasite interactions, modification of the PV, and establishment of intravacuolar network (IVN) of highly curved nanotubules (39). The latter is involved in connecting tachyzoites in the PV and in the salvage of lipids (40, 41) and cytosolic proteins (42) from the host. Some of the GRA proteins, especially those associated with the IVN network (GRA2, GRA6, GRA4, and GRA12), relocalize to the forming cyst wall and impact CST1 localisation (38). Of these, GRA2 is essential for IVN formation (43), acute virulence and cyst formation (44, 45), yet details of its function during the chronic stage remain unclear. GRA2 appears to have a dynamic cyst wall localization being present in early cysts at day 7 (D7) and D10, with its location overlapping with the CST1 signal (38), while absent from the wall on late cysts (46).

Here, we apply U-ExM to *Toxoplasma* tissue cysts produced *in vitro* demonstrating that the original protocols do not successfully expand these structures. This problem is solved by the addition of an enzymatic digestion step with mucin-selective protease StcE (47), during the sample preparation. StcE cuts through the mucin domains of the major structural protein of the cyst wall CST1, allowing the cyst to expand fully, without damaging CST1 or other protein epitopes. We used this method to assess the co-localisation of CST1 and GRA2 in the cyst wall and observed distinct localisation at this higher resolution. The addition of the StcE step to the U-ExM protocol opens new avenues to precisely localize proteins in bradyzoites, as exemplified here with the proteins associated with the cyst wall, to aid in understanding their role in cyst formation and growth.

Materials and methods

Cell culture

Primary human foreskin fibroblasts (HFFs) (ATCC) were maintained in Dulbecco's modified Eagle's medium (DMEM, Sigma-Aldrich) with 4.5 g/L glucose, 25 mm HEPES and 1% v/v GlutaMAX (Gibco) supplemented with 10% v/v fetal bovine serum (FBS, Gibco) at 37°C with 5% CO2.

Parasite strains and culture

Toxoplasma gondii ME49Δ*ku80*Δ*hxgprt (48)* and 76K tachyzoites were propagated *in vitro* in HFFs using DMEM supplemented with 2% v/v heat-inactivated FBS, 1% v/v glutaMAX, and 1% v/v penicillin-streptomycin solution (Gibco). Tachyzoites were grown in ventilated tissue culture flasks at 37°C and 5 % CO2. Prior to infection, intracellular parasites were isolated by syringe passage with 23-gauge blunt needles (SAI Infusion Technologies) and filtration through a 5 µm membrane filter (Sartorius).

Parasite infections

For confocal and U-ExM imaging, HFFs were seeded on 13-mm no. 1.5 coverslips (SLS) in 24-well plates. Confluent monolayers at least 7 days old were infected at a multiplicity of infection (MOI) of 1 for 24 hours. Cells were fixed in 4% formaldehyde (FA, Thermo Scientific) for 15 min at RT.

Conversion to bradyzoites

Bradyzoite cultures were obtained by infecting HFF monolayers coverslips with tachyzoites at an MOI of 1 for 3.5 hours, followed by media change to filtered RPMI 1640 media (Sigma-Aldrich) supplemented with 1% v/v FBS, and 50mM HEPES (Sigma-Aldrich) and brought to pH 8.2. The bradyzoite culture was grown with ambient CO2 at 37°C for 7 days with daily media changes. Cells were fixed in 4% FA for 15 min at RT.

T. gondii infection of primary neuronal culture obtained from the hippocampus of postnatal rats was performed as described previously (33). Briefly, after the dissection of the brains, hippocampi were mechanically dissociated and resuspended in Neurobasal A, a medium supplemented with GlutaMAX and B27 neural supplement with antioxidants (Gibco). Cells were plated at a density of 100 000 cells/cm^2 in poly-L-lysine coated 24-well plates containing coverslips. Brain cells were grown for 14 days before infection. Each well was infected by 1.10^4 tachyzoites of the 76K strain resuspended in the Neurobasal A medium. The culture was grown for an extra 14 days to obtain fully mature cysts as described in Mouveaux *et al*.

Standard immunofluorescence assays

For immunofluorescence assays, fixed cells were permeabilised with 0.1% Triton X-100 (Sigma-Aldrich) in PBS for 2 min at RT for tachyzoites or 0.2% Triton X-100, 0.1% glycine (Sigma-Aldrich), and 0.2% BSA in PBS for 20 min on ice for bradyzoites. Samples were then incubated in blocking solution (2% BSA in PBS) for 1 hour, followed by 45 min incubation with antibodies/stains (diluted in blocking solution).

Infected cells, depending on experiment, were stained using antibodies and dyes listed in **Table 1**. Coverslips were washed three times after primary and secondary antibody/stain incubations, and coverslips were subsequently washed and mounted with Vectashield Antifade softset mountant (H-1000; Vector Laboratories). Parasites were visualized on a Zeiss LSM980 laser confocal microscope.

Ultrastructure expansion microscopy (U-ExM)

Gambarotto and colleagues published a detailed U-ExM protocol in 2021 (49). For reagents list, see **Table 1**. Briefly, fixed infected HFFs or primary neuronal cultures on coverslips were first permeabilised (tachyzoites: 0.1% Triton X-100 in PBS for 2 min at RT; bradyzoites: 0.2% Triton X-100, 0.1% glycine, and 0.2% bovine serum albumin (BSA) in PBS for 20 min on ice). They were then incubated in protein crosslinking prevention solution (final conc. 1.4% PFA/2% Acrylamide (AA)) at 37°C with no shaking overnight.

To obtain fully expanded cysts, protein crosslinking prevention was followed by the incubation with 100nM StcE mucinase in PBS (gift from Kayvon Pedram, (50)) for 4 hours at 37°C with no shaking. StcE is also commercially available (SAE0202, Merk). Coverslips were briefly washed 3x PBS and prepared for gelation.

The gelation solution consisted of a monomer solution, topped up with TEMED (Sigma-Aldrich) and APS (Sigma-Aldrich) solutions just before the sample application (**Table 2**). All components except PBS were stored at -20°C and kept on ice just before the application.

The gelation chamber was adapted from (51) and was prepared as follows. A clean press-to-seal silicone isolator (13mm diameter x 0.8mm depth, JTR13R-1.0, Sigma-Aldrich) was mounted on a parafilm-wrapped glass slide. The device was put on a wetted piece of white roll paper, stretched in a plastic chamber (eg. a 24-well plate lid), placed for 5 minutes in -20°C freezer and then kept on ice.

120 µL of fresh gelation solution was placed into the well created by silicon isolator. Immediately after, the sample coverslip was dabbed from excess PBS and placed cells down on the top of the well. The gelation chamber was left for 5 min on ice to aid monomer permeation, and then placed into 37°C incubator for 1 hour for polymerisation.

Once polymerised, the silicone isolator was peeled off, coverslips lifted from the parafilm-covered glass using tweezers, put in 6-well plate (1 gel/well), topped with 2mL denaturation solution (**Table 2**) and left for 15 min on a rocker. By the end of 15 min, gels that were detached from the coverslips were placed in in a 1.5mL Eppendorf tube with the fresh denaturation solution and incubated for 1.5 hours at 95°C in a heating block with no shaking. If gels were not detached by that point, they were left for another 5-10 min on the rocker. After denaturation, gels were then expanded in 250-300mL ddH2O overnight.

The next day, gels underwent 2x15min incubation in PBS (no shaking) to shrink in size, and then cut to the needed shape using scalpel blade (to fit a well in 24-well plate). Note that the gels shrink further during the staining process. Gels were then blocked for 1 hour in a blocking solution (2% BSA in PBS) at 37°C while shaking, and then incubated with the primary and secondary antibodies or stains for 2.5 hours in the same conditions, with 3x10min washes in PBS-0.1%Tween20 solution on a rocker at RT in between incubation steps.

Infected cells, depending on experiment, were stained using antibodies and dyes listed in **Table 1**. Parasites were visualized on a Nikon Ti2 CSU-W1 Spinning Disk microscope or a Zeiss LSM980 laser confocal microscope in 35-mm high glass-bottom petri µ-dishes (Ibidi), covered in-house with Poly-D-lysine (Thermo Scientific) for 1h, followed by 3x ddH2O washes, and then dried.

Image acquisition

Imaging was performed in Centre Optical Instrumentation Laboratory (COIL), University of Edinburgh. Two microscopes were used to visualise expanded samples: Nikon Ti2 CSU-W1 Spinning Disk Confocal (objective: 100x: Plan Apo TIRF, Oil, 1.45 NA) and Zeiss LSM980 laser-scanning confocal

189 microscope (objectives: 20x: Plan Apochromat, Air, 0.8 NA; 100x: Alpha Plan Apochromat, Oil, 1.45
190 NA, DIC). Initially Nikon Ti2 CSU-W1 Spinning Disk Confocal was used for faster gel imaging to avoid
191 potential gel drift. However, poly-D-lysine covering substantially reduced the drift when imaged on
192 more sensitive Zeiss LSM980 laser-scanning confocal microscope, and thus, all consequent imaging
193 was performed using Zeiss.

194 ## Image Processing and Data Analysis

195 The images were exported using either Zen Blue software (Zeiss) or ImageJ. The brightness was
196 adjusted for display purposes, but the measurements were taken on raw unprocessed files.

197 The expansion factor was determined by the comparison of the average cross-section length of
198 parasite nuclei stained with DAPI nuclear stain (along the longest axis) in the tachyzoites before and
199 after expansion. Data analysis and statistical tests (t-tests) were performed in GraphPad Prism
200 software.

201

202

203

204 **Table 1. Key resources table**

Category	Reagents	Manufacturer	Additional information
U-ExM protocol reagents	Acrylamide, 40% (AA)	Sigma-Aldrich	
	Ammonium persulfate (APS)	Sigma-Aldrich	
	Formaldehyde, 37% (FA)	Sigma-Aldrich	
	N,N'-methylenbisacrylamide, 2% (Bis)	Sigma-Aldrich	
	Sodium Chloride (NaCl)	Thermo Fisher	
	SDS, 20%	ThermoFisher	
	Sodium Acrylate (SA)	AKSci	
	TEMED	Sigma-Aldrich	
	Tris base	ThermoFisher	
	Tween20	Sigma-Aldrich	
	Poly-D-lysine	Thermo Scientific	
	StcE mucinase, 20 uM	Gift from Kayvon Pedram, (50)	Commercially available from Merk, Cat N SAE0202
Dyes, stains, antibodies, and mountants	DAPI (4',6 Diamidino 2 Phenylindole, Dilactate)	Invitrogen	1:1000 (std), 1:100 (ExM)
	Dolichos Biflorus Agglutinin (DBA), biotinylated	Vector Laboratories	1:2500 (std), 1:1000 (ExM)
	anti-GRA2 mouse	Biotem	1:1000 (std), 1:300 (ExM)
	anti-SAG1 rabbit	Abcam	1:1000 (std)
	anti-CST1 rabbit	Gift from L. Weiss, (30)	1:200 (std), 1:100 (ExM)
	anti-TgGAP45 rabbit	Gift from D. Soldati-Favre, (52)	1:10000 (std), 1:7000 (ExM)
	AlexaFluor 488 goat anti-mouse superclonal	Thermo Scientific	1:1000 (std), 1:300 (ExM)
	AlexaFluor 568 goat anti-mouse	Thermo Scientific	1:1000 (std), 1:300 (ExM)
	AlexaFluor 488 goat anti-rabbit	Thermo Scientific	1:1000 (std), 1:300 (ExM)
	AlexaFluor 568 goat anti-rabbit	Thermo Scientific	1:1000 (std), 1:300 (ExM)
	Atto 647N goat anti-rabbit	Sigma-Aldrich	1:1000 (std), 1:300 (ExM)
	NHS ester, Atto 565 conjugate	BioReagent	1:300 (std), 1:300 (ExM)
	Streptavidin, AlexaFluor 488 conjugate	Invitrogen	1:1000 (std), 1:300 (ExM)
	Streptavidin, AlexaFluor 568 conjugate	Invitrogen	1:1000 (std), 1:300 (ExM)
	Mounting media VECTASHIELD Antifade	Vector Laboratories	
Tissue culture media and reagents	Dulbecco's modified Eagle's medium	Thermo Fisher	
	RPMI 1640 media	Sigma-Aldrich	
	Fetal bovine serum	Thermo Fisher	
	Bovine serum albumin	Sigma-Aldrich	
	HEPES	Sigma-Aldrich	

	Penicillin-streptomycin solution	Thermo Fisher	
	GlutaMAX	Thermo Fisher	
	Formaldehyde, 16%	ThermoFisher	
	Glycine	Sigma-Aldrich	
	Triton X-100	Sigma-Aldrich	
Tissue culture and staining consumables	Blunt needles 23G	SAI Infusion Technologies	
	Cellulose Acetate membrane filter, 5 µm	Sartorius	
	Coverslips No 1.5, Dia 13 mm	SLS	
	Press-to-seal silicone isolator (13mm*0.8mm)	Sigma-Aldrich	
	35-mm high glass-bottom petri µ-dishes	Ibidi	

Table 2. Expansion microscopy buffers

FA/AA mix in PBS		
Reagent	**Stock, %**	**Final, %**
PFA	37	1.4
AA	40	2

Monomer solution		
Reagent	**Stock, %**	**Final, %**
SA	38	19
AA	40	10
BIS	2	0.1
PBS	10x	1x

StcE mucinase enzyme		
Reagent	**Stock, uM**	**Final, uM**
StcE	20	0.1

Gelling solution top-up 1		
Reagent	**Stock, %**	**Final, %**
TEMED	100	10

Denaturation buffer		
Reagent	**Stock, mM**	**Final, mM**
SDS	350	200
NaCl	5000	200
Tris	1000	50
H2O	Fill up to the needed volume	

Gelling solution top-up 2		
Reagent	**Stock, %**	**Final, %**
APS	100	10

210

Results

Standard Ultrastructure Expansion Microscopy protocol does not fully expand *T. gondii* cysts

Standard U-ExM protocols have been successfully applied to extracellular *Toxoplasma* and tachyzoites within infected cells (reviewed in (3)). To assess whether this method could be applied to *Toxoplasma* cysts, we first compared U-ExM protocol on *Toxoplasma* infected cells grown under standard conditions (tachyzoites) or under pH stress to induce conversion to bradyzoites.

The standard U-ExM protocol of expansion *T. gondii* parasites from a monolayer of infected cells takes three days (**Fig.1A**) and consists of the following steps: fixation and permeabilisation of the tissue, incubation in crosslinking preventative and protein anchoring solution, gelation and polymerisation, followed by denaturation at 95^{o}C with 200mM SDS, antibody labelling and final expansion of the gelled sample in water (2, 49).

For the tachyzoite samples, the expansion was successful (**Fig.1B-E**) with an average expansion factor of 4.3x (**Fig.1C**), similar to the published values of 4-4.3x for *T. gondii* (10, 23, 53) *Plasmodium falciparum*, and *Cryptosporidium parvum parasites* (3).

NHS ester binds all proteins, and its fluorophore-conjugated version was used to visualise the cell architecture, which demonstrated that the host-cell environment tightly surrounds the PV in the expanded sample, leaving no gap (**Fig.1E, white arrows**). In contrast, when comparing the expanded and non-expanded *T. gondii* cysts of D7 bradyzoite culture with anti-CST1 antibody used as a cyst wall marker (**Fig.1F-G**), a large black gap was consistently visible between the cyst and the surrounding tissue of the expanded host cell (**Fig. 1G**). Furthermore, quantification of the bradyzoite nuclei cross-section before and after expansion revealed a smaller 2.5x expansion factor compared to 4.3x in tachyzoite samples (**Fig.1C**), rendering the standard U-ExM protocol insufficient for super-resolution studies of the *Toxoplasma* cyst wall.

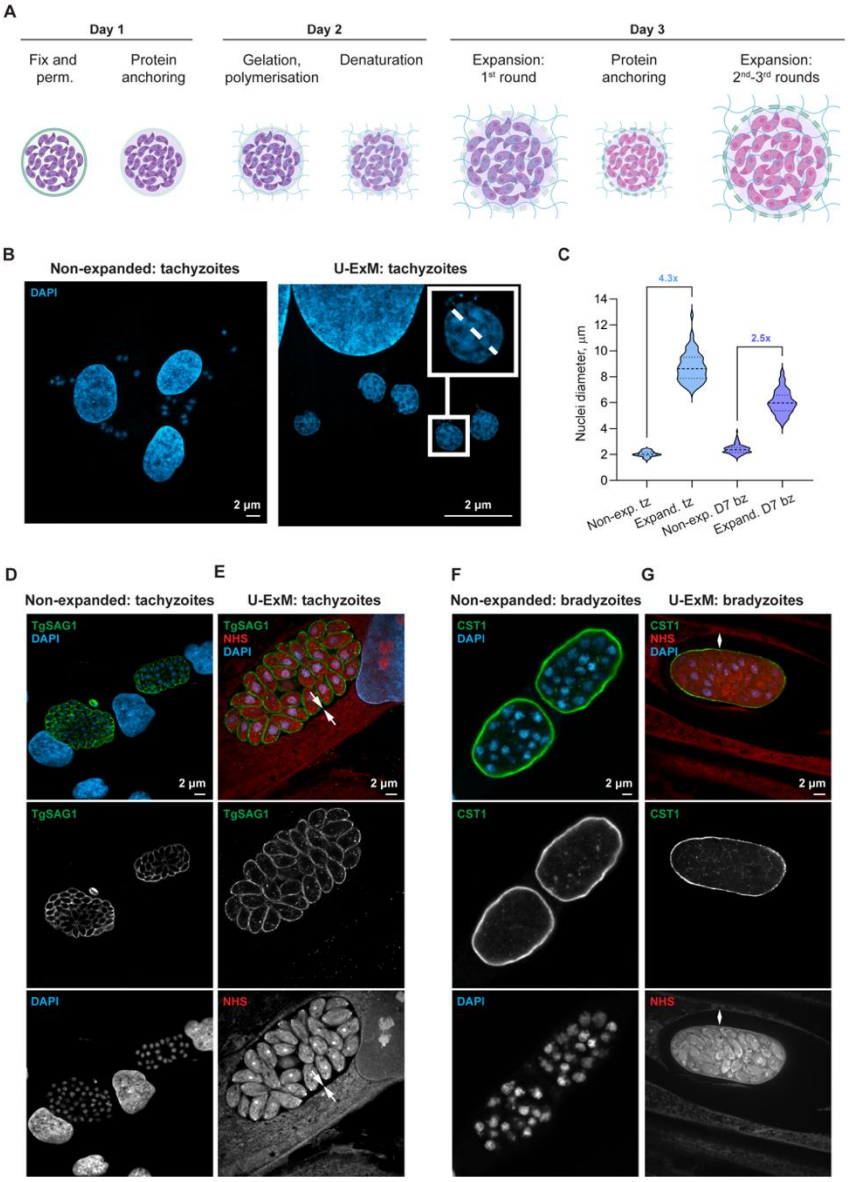

Figure 1. Standard U-ExM protocol expands intracellular *T. gondii* tachyzoites but fails to expand the cyst wall

(A) An overview of the standard U-ExM protocol workflow (created with BioRender.com). **(B)** Confocal images of HFF monolayer infected with Type II ME49Δku80Δhxgprt tachyzoites, fixed 24h pi, and labelled with DAPI nuclear stain. Large nuclei belong to host cells, smaller are tachyzoite nuclei. Insert shows the example of tachyzoite nuclei measurement along its longest diameter to calculate the expansion factor of the U-ExM sample. **(C)** The expansion factor was determined by comparison of the average cross-section of tachyzoite (light blue) and bradyzoite (violet) nuclei stained with DAPI in non-expanded samples versus U-ExM-processed. The tachyzoite expansion factor is 4.3x, while only 2.5x for bradyzoites (for both unpaired t-test, $p < 0.0001$) ($n_{non\text{-}exp.\ tz}$= 79, $n_{exp.\ tz}$=131, $n_{non\text{-}exp.\ bz}$=201, $n_{exp.\ bz}$=112). **(D,E)** Immunofluorescence images of HFFs infected with ME49Δku80Δhxgprt tachyzoites for 24h. Confocal images (single optical sections) of non-expanded tachyzoites in (D) versus U-ExM-processed shown in (E), both probed with anti-TgSAG1 antibody (green) and DAPI (blue), while U-ExM-processed samples were also stained with all-protein NHS-565 dye (red). White arrows indicate continuous host-cell environment surrounding the parasitophorous vacuole. **(F,G)** Immunofluorescence images of ME49Δku80Δhxgprt infected HFFs grown under bradyzoite inducing conditions for 7 days. Confocal images (single optical sections) of non-expanded D7 cysts in (F), versus U-ExM-processed shown in (G). Both samples were probed with anti-CST1 antibody (green) and DAPI (blue), while U-ExM-processed samples were also stained with all-protein conjugated NHS-565 dye (red). White arrows show a gap between the fully expanded host cell and only partially expanded cyst. Tz – tachyzoites, Bz – bradyzoites, exp. – expanded.

Incubation with the mucin-selective protease StcE prior U-ExM processing allows full expansion of the *T. gondii* cyst in fibroblasts and primary neurons

It is well established that the *Toxoplasma* cyst wall consists of an enrichment of glycoproteins including CST1, SRS13, and TgPPG (30, 54, 55). Of these, CST1 is a major structural component of the cyst, and is a SAG1-related sequence protein with a heavily glycosylated mucin domain (30). We initially addressed the problem of partially expanding cysts by attempting enzymatic digestion using Proteinase K (ProK), commonly used in protein retention expansion microscopy (pro-ExM), alongside the denaturation step (data not shown). However, carbohydrate modifications of the cyst wall were resistant to this type of proteolytic digestion. As an alternative enzymatic approach that would disrupt densely packed glycosylated domains without reducing protein signals, we included a mucinase StcE step in the protocol. StcE is a mucin-selective protease with a specific peptide- and glycan-based cleavage motif that digests the mucin domain, as shown in **Figure 2A,B** (47). We first tested whether the StcE enzyme affects the proteins associated with the cyst wall in a non-expanded sample (**Fig. 2C**) by introducing a StcE enzymatic treatment after the permeabilisation step. Cysts from the D7 bradyzoite culture labelled with antibodies against CST1 and GRA2 show the expected protein localisations after 4h incubation with StcE at 37°C, showing that it doesn't destroy the cyst wall. In fact, both signals increased in intensity following the StcE step, possibly as a result of increased antibody accessibility.

We then introduced StcE treatment after the permeabilization step in the U-ExM protocol. With this optimised protocol we observed successful expansion of 7-day *Toxoplasma* cysts with an expansion factor of 4.x **(Fig. 2D)**, similar to that of tachyzoites. Crucially, no gap is observed between the expanded cyst and the host cell environment (**white arrows, Fig. 2E)**.

It was recently shown by Mouveaux et al., that D14 *in vitro* cysts were able to infect a mouse following oral gavage, while infection with D7 cysts was unsuccessful (33). This may be that the cyst wall continues to mature and becomes more robust over time, or that the parasites differentiate further. In order to verify the StcE enhanced U-ExM protocol on infectious cysts, we tested 14-day old cysts generated in primary neuronal cultures from postnatal rat hippocampus alongside with the D7 cysts from the HFF monolayer. Reassuringly, a similar expansion factor was observed **(Fig. 2D)**, with no gap between the packed cyst structure and the surrounding cell **(Fig. 2E)**. To further assess the method, expanded *in vitro* cysts were probed with antibodies against the inner membrane complex, GAP45, and the secreted protein GRA2 along with anti-CST1 for the cyst wall **(Fig. 3A-D)**. All antibodies showed their expected localisation patterns, with GAP45 outlining the parasite shape, and GRA2 split between intracellular staining within dense granules and localised around the periphery of the cyst.

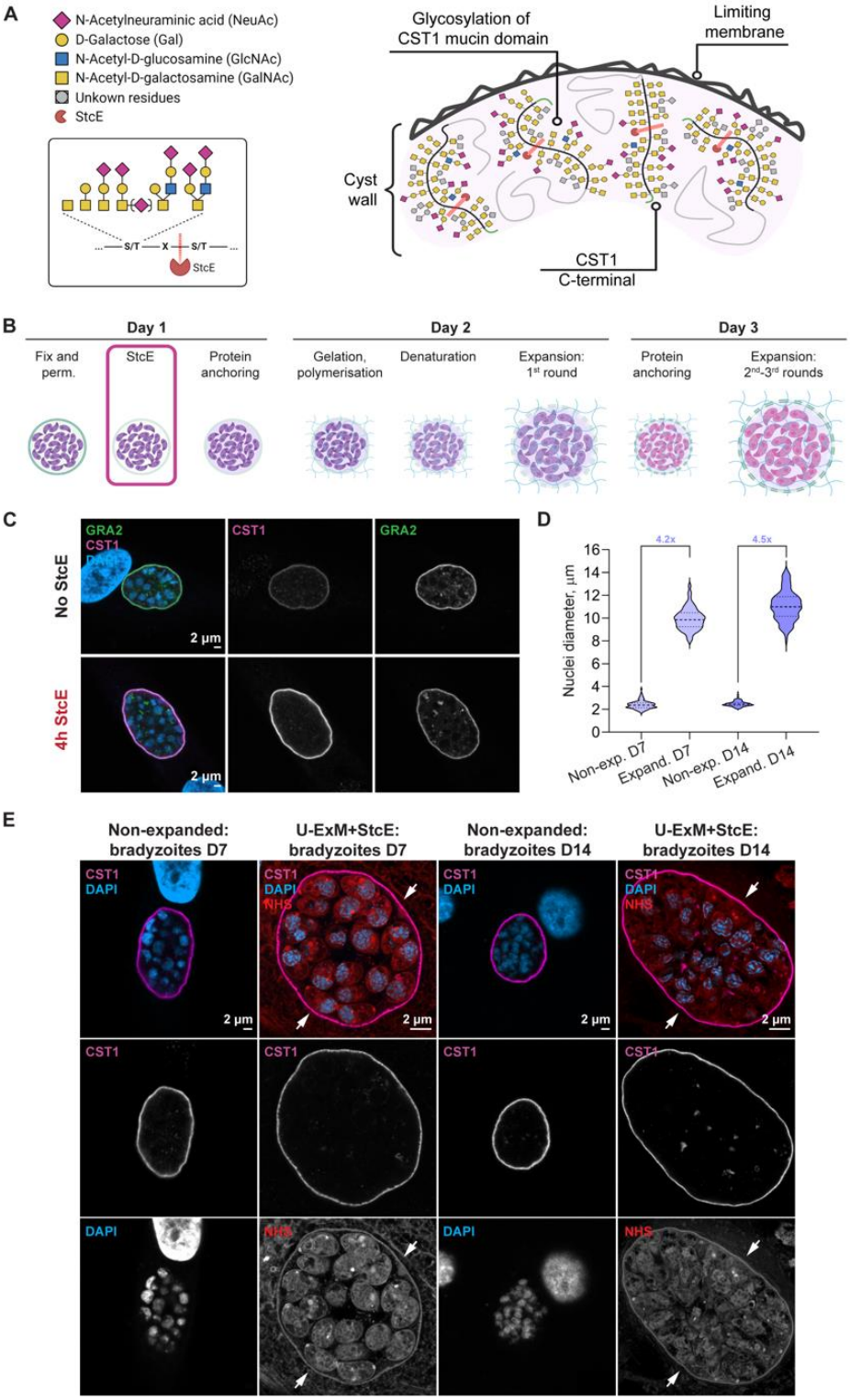

Figure 2. U-ExM protocol complemented with StcE digestion fully expands the cyst wall of D7 and D14 cysts.

(A) Proposed mechanism of mucin domain cleavage by StcE mucin-selective protease. Diagram shows part of the cyst wall, depicting the limiting membrane (faces host-cell environment), and the CST1-positive layer with the ribbon-like glycoprotein structures of CST1 mucin domains. The glycoprotein structures illustrated in the cyst wall diagram correspond to those known to be associated with CST1 (featuring GalNAc-GalNAc as a DBA-binding site (30, 36)), and those that are preferred cleavage targets of StcE. Insert depicts the StcE cleavage point on the glycopeptide chain. StcE cleaves before the second S/T within the motif S/T*–X–S/T, where the

asterisk indicates modification with a glycan and X can be any amino acid or absent (47). **(B)** Adapted U-ExM protocol workflow with added StcE enzymatic treatment (100 nM, 4h, 37°C, no shaking) after the permeabilization step. **(C)** Representative confocal images (single optical sections) of non-expanded HFF monolayer infected with Type II ME49Δku80Δhxgprt D7 cysts with and without StcE treatment. Samples were labelled with antibodies against GRA2 (green), CST1 (magenta), and stained with DAPI nuclear stain, followed by imaging under the identical acquisition settings. *Top row*: no StcE treatment (control); *bottom row*: samples treated with 4h StcE at 37°C after permeabilization step. **(D)** The expansion factor of 4.2x was determined by the comparison of the average cross-section length of D7 bradyzoite nuclei in CST1-labelled cysts stained with DAPI in non-expanded HFF samples versus U-ExM+StcE-processed HFFs (unpaired t-test, $p < 0.0001$), and 4.5x in non-expanded neurons versus U-ExtM+StcE processed neurons (unpaired t-test, $p < 0.0001$) ($n_{\text{non-exp.bz HFFs}} = 201$, $n_{\text{non-exp.bz neurons}} = 218$, $n_{\text{exp.bz HFFs}} = 185$, $n_{\text{exp.bz neurons}} = 123$). **(E)** Confocal images (single optical sections) of non-expanded D7 (in HFFs) and D14 cysts (in neurons) versus expanded using U-ExM+StcE. All samples were probed with anti-CST1 (magenta) antibody and DAPI (blue), with the additional all-protein NHS-565 stain (red) for U-ExM+StcE. White arrows indicate continuous host-cell environment surrounding cyst wall. Tz – tachyzoites, Bz – bradyzoites, exp. – expanded. Diagrams in panels (A) and (B) created with BioRender.com.

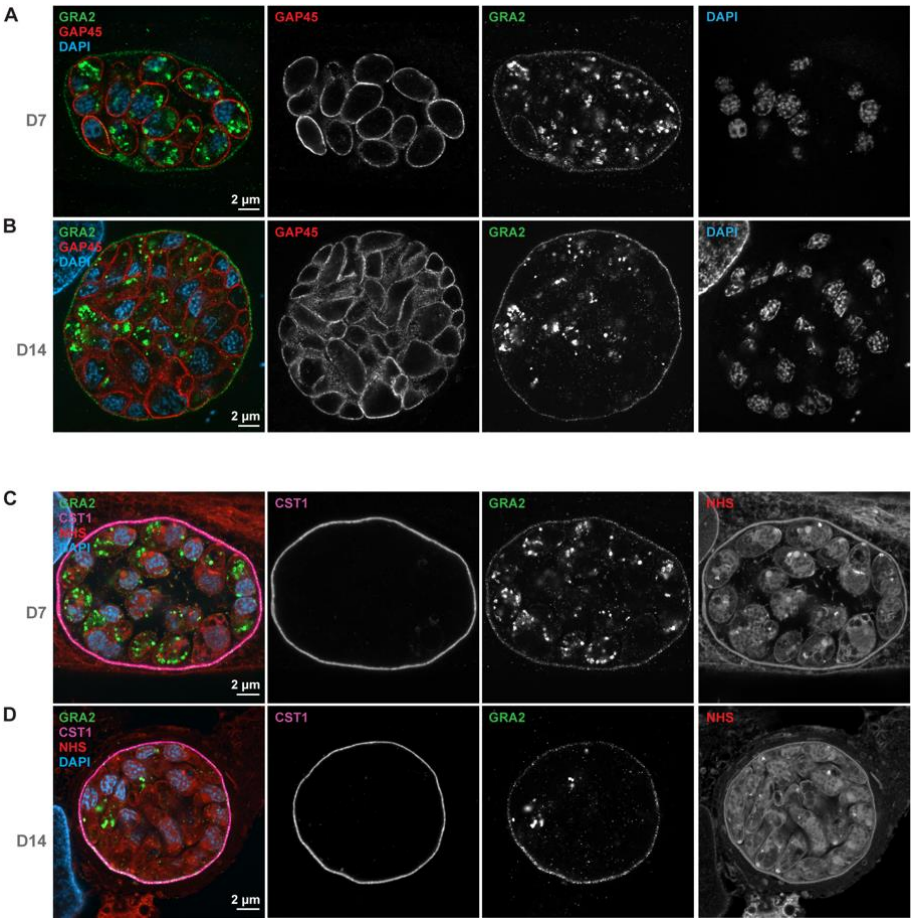

Figure 3. U-ExM+StcE protocol preserves protein signals in *T. gondii* cysts *in vitro* (D7 fibroblasts, D14 neurons)

(A-B) Confocal image (single optical section) of the U-ExM+StcE-expanded HFF monolayer with Type II ME49Δku80Δhxgprt D7 cyst **(A)** and primary neuronal culture (derived from P0 rat hippocampus) with Type II 76K D14 **(B)** cyst at 100x magnification. Samples were labelled with antibodies against GRA2 (green), GAP45 (magenta), biotinylated DBA (not shown), and stained with DAPI nuclear stain. Each row consists of a merged image on the left, followed by separate channels in grey. **(C-D)** Confocal image (single optical section) of the U-ExM+StcE-expanded HFF monolayer with Type II ME49Δku80Δhxgprt D7 cyst **(C)** and primary neuronal culture (derived from P0 rat hippocampus) with Type II 76K D14 **(D)** cyst at 100x magnification. Samples were labelled with antibodies against GRA2 (green), CST1 (magenta), and stained with NHS-565 and DAPI.

Modified U-ExM-StcE protocol reveals that GRA2 is only partially localised to the CST1-positive layer in the cyst wall

While many proteins secreted from the dense granules are known to localise to the cyst wall (46, 56, 57), current microscopy techniques have not allowed more detailed visualisation of substructures. We therefore used the U-ExM+StcE protocol to clarify the location of GRA2 relative to CST1 protein in the *T. gondii* cyst wall in HFFs (D7) and primary rat neuronal cultures (D14). While previous data has shown smooth overlapping signal for CST1 and GRA2 in *in vitro* cysts (38), we observe a more granular distribution of GRA2 in the cyst wall compared to the smooth signal of CST1 with StcE enhanced U-ExM (**Fig.4A**). The GRA2 granules in the expanded cyst are observed on both the outer and inner sides of the CST1 layer, with enrichments visible on the inner side of the wall (**Fig. 4B-E**). In viewing the z-stack of images through the wall these GRA2 structures appear to span through the

CST1-positive layer **(Supp Movie 1)**. A similar pattern was observed in D14 cysts from infected primary neuronal cultures (**Fig.4 F-J**).

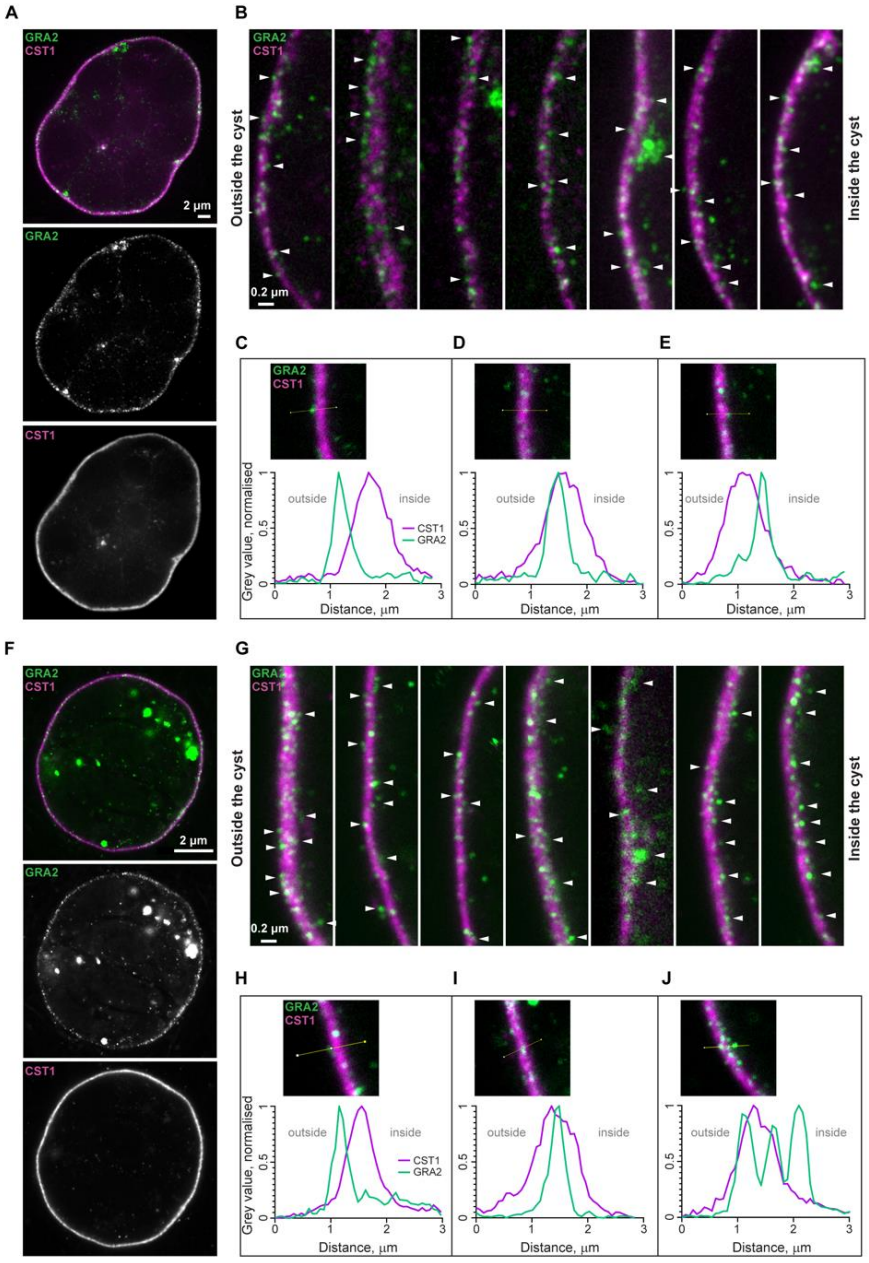

Figure 4. U-ExM of *in vitro* cysts shows GRA2 spanning the CST1-positive layer in HFF D7 and neuronal D14 *T. gondii* culture

(A) Confocal image of the U-ExM+StcE-expanded HFF monolayer with Type II ME49Δku80Δhxgprt D7 cyst at 100x magnification (single optical section of the widest cross-section of the cyst). Sample wase labelled with antibodies against GRA2 (green) and CST1 (magenta). **(B)** Zoomed cyst-wall regions of the three D7 cysts. White arrows highlight examples GRA2 puncta inside and outside the CST1 layer. **(C-E)** Fluorescence intensity profiles showing different locations of GRA2 relative to CST1 in a single U-ExM+StcE-expanded D7 cyst grown in HFF monolayer. Normalised intensity levels (grey values) obtained from the raw images were plotted against the length of the sampled area (yellow line, image insert). **(C)** GRA2 localises outside the CST1 layer, on the exterior side of the cyst wall, facing host-cell environment. **(D)** GRA2 fully co-localises with CST1. **(E)** GRA2 localises outside the CST1 layer, on the interior side of the cyst wall facing cyst matrix. **(F)** Confocal image of

the U-ExM+StcE-expanded primary neuronal culture (derived from P0 rat hippocampus) with Type II 76K D14 cyst at 100x magnification (single optical section of the widest cross-section of the cyst), presented as in (A). **(G)** Zoomed cyst-wall regions of the three D14 cysts. White arrows show GRA2 puncta inside and outside the CST1 layer. See also Supp Movie 1. **(H-J)** Fluorescence intensity profiles showing different locations of GRA2 relative to CST1 in a single U-ExM+StcE-expanded Type II 76K D14 cyst grown in a primary neuronal culture. Normalised intensity levels (grey values) obtained from the raw images were plotted against the length of the sampled area (yellow line, image insert). **(H)** GRA2 localises outside the CST1 layer, on the exterior side of the cyst wall facing host cell environment. **(I)** GRA2 fully co-localises with the CST1. **(J)** Three GRA2 punctae localise across the CST1 layer: one on the exterior side of the cyst wall, one in the middle of CST1-positive layer, and one outside, facing cyst matrix.

Discussion

Despite the importance of chronic *Toxoplasma* cysts in transmission and their reactivation in human disease, the detailed structure of the cyst is yet to be clarified. While EM has provided key insights into the wall morphology, resolution has limited the ability to precisely localise many cyst wall proteins. A relatively new modification of the sample expansion technique, U-ExM, is an easy, cost-effective alternative to the established super-resolution approaches, allowing direct mapping of the sample morphology to protein location.

When attempting to use U-ExM for cyst wall protein localisation, we discovered that the standard U-ExM protocol fails to expand the cyst wall up to the expected 4-4.3x expansion factor. The addition of the enzymatic step targeting glycosylated mucin domains of CST1 and, potentially, SRS13 proteins using StcE mucinase solves the ineffective expansion, allowing protein localisation studies in fully expanded cysts. We confirmed our results in Day 7 and Day 14 cysts grown in HFF monolayers and primary rat neuronal cell culture, respectively.

We then used the technique to clarify the location of the GRA2 protein relative to the CST1-positive layer in the cyst wall. Previously published studies based on standard confocal images show full co-localisation of GRA2 and CST1 both appearing as a smooth signal across the cyst wall (38). Using modified U-ExM+StcE protocol, we show that GRA2 is distributed as puncta across the still smooth CST1-positive layer, which was consistent in both in D7 *Toxoplasma* cysts in fibroblasts and and D14 cysts in neurons *in vitro*. Moreover, fully expanded cysts show GRA2 spanning the CST1-positive layer, providing previously unknown details about the GRA2 location in the *Toxoplasma* cyst. Enrichments of GRA2 signal were observed underneath the CST1 layer, with putative spirals going through the CST1 layer. In the future, it will be interesting to investigate if these represent clusters of tubular network of the IVN and colocalise with other GRAs.

Early work on GRA2 localisation using immuno-electron microscopy with labelled golden particles, showed GRA2 secretion from the tachyzoites into the PV lumen and its association with the IVN, although the GRA2 localization doesn't follow any specific pattern (58). It is well known that GRA2 is essential for the correct organisation of the IVN in tachyzoite PVs (43), and impacts the cyst wall and matrix during the chronic stage (38). This, and its relocation to the cyst wall with the subsequent co-localisation with the major structural protein CST1, suggests that GRA2 retains its role in the organisation of the parasitic structures after the stage conversion, however, its precise function is still unclear.

Although a significant portion of GRA2 relocalises to the cyst wall, some remain in the cyst matrix as puncta (38). Regular (non-expansion) immunofluorescence assays depict cyst-wall-associated GRA2 as a smooth continuous signal. We show that GRA2 retains its puncta appearance in the cyst matrix and the cyst wall.

Despite the growing number of proteins localised to the cyst wall over the past few years (56, 57, 59), we still don't know their functional relevance in the development and maturation of the cyst. By revealing more precise protein localisations, U-ExM+StcE can play a key role in investigating their role by expanding our knowledge of substructures within the wall. Indeed, with the expansion of *Toxoplasma* cysts over time, and their subsequent rupture to release parasites, it is clear that the cyst wall is subject to remodelling.

In conclusion, the U-ExM+StcE protocol is a powerful addition to the microscopy toolbox aimed at the investigation of *in vitro Toxoplasma* cysts with nanoscale resolution, joining other recent efforts to adapt expansion protocols for non-mammalian samples via tailored enzymatic disruption (60). In our case, the simplicity of a single-enzyme treatment with a pan-mucinase (50) to break down the mucin-rich glycocalyx of the *Toxoplasma* cyst wall underscores the importance of biochemical characterization of structural biomolecules for successful Expansion Microscopy.

Acknowledgments

We thank all members of the Young lab as well as Nisha Philip and Joanne Thompson for critical discussion and support. We particularly thank Johanna Dornell for technical assistance on HFF culture. We thank Paul Tillberg (Janelia Research Campus) for advice on enzymatic digestion and for referring us to Kayvon Pedram. We also thank Dominique Soldati-Favre (University of Geneva, Switzerland) for providing anti-GAP45 antibody, and Louis Weiss (Albert Einstein College of Medicine, USA) for providing anti-CST1 antibody. This work was funded by an MRC Career Development award (MR/V03314X/1) supporting JCY and KB. MG is a CNRS researcher. MG and FL were supported by a Transdisciplinary Research Projects grant from the Pasteur Institute in Lille awarded to MG. Imaging was performed in Centre Optical Instrumentation Laboratory (COIL), which is supported by funding for the Wellcome Discovery Research Platform for Hidden Cell Biology [226791] and we gratefully acknowledge support from the Microscopy core, particularly David Kelly and Toni Mchugh for training and technical assistance. The use of Nikon Ti2 CSU-W1 Spinning Disk and Zeiss LSM980 confocal microscopes was supported by the Wellcome Trust grant [203149].

Data availability

All data is freely available upon request.

Open Access Statement

Competing Interest Statement

Authors declare no competing interests.

436 # References

437 1. Chen F, Tillberg PW, Boyden ES. 2015. Expansion microscopy. Science 347:543–548.

438 2. Gambarotto D, Zwettler FU, Le Guennec M, Schmidt-Cernohorska M, Fortun D, Borgers S,
439 Heine J, Schloetel J-G, Reuss M, Unser M, Boyden ES, Sauer M, Hamel V, Guichard P. 2019.
440 Imaging cellular ultrastructures using expansion microscopy (U-ExM). Nat Methods 16:71–74.

441 3. Liffner B, Absalon S. 2023. Expansion microscopy of apicomplexan parasites. Mol Microbiol
442 https://doi.org/10.1111/mmi.15135.

443 4. Asano SM, Gao R, Wassie AT, Tillberg PW, Chen F, Boyden ES. 2018. Expansion Microscopy:
444 Protocols for Imaging Proteins and RNA in Cells and Tissues. Current Protocols in Cell Biology
445 80:e56.

446 5. Bertiaux E, Balestra AC, Bournonville L, Louvel V, Maco B, Soldati-Favre D, Brochet M, Guichard
447 P, Hamel V. 2021. Expansion microscopy provides new insights into the cytoskeleton of malaria
448 parasites including the conservation of a conoid. PLOS Biology 19:e3001020.

449 6. Pavlou G, Touquet B, Vigetti L, Renesto P, Bougdour A, Debarre D, Balland M, Tardieux I. 2020.
450 Coupling Polar Adhesion with Traction, Spring, and Torque Forces Allows High-Speed Helical
451 Migration of the Protozoan Parasite Toxoplasma. ACS Nano 14:7121–7139.

452 7. Dave N, LaFavers K, Arrizabalaga G. 2022. The Dually Localized EF-Hand Domain-Containing
453 Protein TgEFP1 Regulates the Lytic Cycle of Toxoplasma gondii. Cells 11:1709.

454 8. Lentini G, Ben Chaabene R, Vadas O, Ramakrishnan C, Mukherjee B, Mehta V, Lunghi M,
455 Grossmann J, Maco B, Visentin R, Hehl AB, Korkhov VM, Soldati-Favre D. 2021. Structural
456 insights into an atypical secretory pathway kinase crucial for Toxoplasma gondii invasion. Nat
457 Commun 12:3788.

458 9. Engelberg K, Bechtel T, Michaud C, Weerapana E, Gubbels M-J. 2022. Proteomic
459 characterization of the Toxoplasma gondii cytokinesis machinery portrays an expanded
460 hierarchy of its assembly and function. Nat Commun 13:4644.

461 10. Louvel V, Haase R, Mercey O, Laporte MH, Eloy T, Baudrier É, Fortun D, Soldati-Favre D, Hamel
462 V, Guichard P. 2023. iU-ExM: nanoscopy of organelles and tissues with iterative ultrastructure
463 expansion microscopy. Nat Commun 14:7893.

464 11. Montano H, Anandkrishnan R, Carruthers VB, Gaji RY. 2023. TgTKL4 Is a Novel Kinase That Plays
465 an Important Role in Toxoplasma Morphology and Fitness. mSphere 8:e00649-22.

466 12. Oliveira Souza RO, Jacobs KN, Back PS, Bradley PJ, Arrizabalaga G. 2022. IMC10 and LMF1
467 mediate mitochondrial morphology through mitochondrion-pellicle contact sites in
468 Toxoplasma gondii. J Cell Sci 135:jcs260083.

469 13. Sparvoli D, Delabre J, Penarete-Vargas DM, Kumar Mageswaran S, Tsypin LM, Heckendorn J,
470 Theveny L, Maynadier M, Mendonça Cova M, Berry-Sterkers L, Guérin A, Dubremetz J-F,
471 Urbach S, Striepen B, Turkewitz AP, Chang Y-W, Lebrun M. 2022. An apical membrane complex
472 for triggering rhoptry exocytosis and invasion in Toxoplasma. EMBO J 41:e111158.

473 14. Tomasina R, Gonzalez FC, Martins-Duarte ÉS, Bastin P, Gissot M, Francia ME. 2022. Separate To
474 Operate: the Centriole-Free Inner Core of the Centrosome Regulates the Assembly of the
475 Intranuclear Spindle in Toxoplasma gondii. mBio 13:e0185922.

476 15. Guérin A, Strelau KM, Barylyuk K, Wallbank BA, Berry L, Crook OM, Lilley KS, Waller RF,
477 Striepen B. 2023. *Cryptosporidium* uses multiple distinct secretory organelles to interact with
478 and modify its host cell. Cell Host & Microbe 31:650-664.e6.

16. John A, M Bader S, Madiedo Soler N, Wiradiputri K, Tichkule S, Smyth ST, Ralph SA, Jex AR, Scott NE, Tonkin CJ, Goddard-Borger ED. 2023. Conservation, abundance, glycosylation profile, and localization of the TSP protein family in Cryptosporidium parvum. J Biol Chem 299:103006.

17. Liffner B, Cepeda Diaz AK, Blauwkamp J, Anaguano D, Frolich S, Muralidharan V, Wilson DW, Dvorin JD, Absalon S. 2023. Atlas of Plasmodium falciparum intraerythrocytic development using expansion microscopy. Elife 12:RP88088.

18. Simon CS, Funaya C, Bauer J, Voβ Y, Machado M, Penning A, Klaschka D, Cyrklaff M, Kim J, Ganter M, Guizetti J. 2021. An extended DNA-free intranuclear compartment organizes centrosome microtubules in malaria parasites. Life Sci Alliance 4:e202101199.

19. Rashpa R, Klages N, Schvartz D, Pasquarello C, Brochet M. 2023. The Skp1-Cullin1-FBXO1 complex is a pleiotropic regulator required for the formation of gametes and motile forms in Plasmodium berghei. Nat Commun 14:1312.

20. Morano AA, Rudlaff RM, Dvorin JD. 2023. A PPP-type pseudophosphatase is required for the maintenance of basal complex integrity in Plasmodium falciparum. Nat Commun 14:3916.

21. Qian P, Wang X, Zhong C-Q, Wang J, Cai M, Nguitragool W, Li J, Cui H, Yuan J. 2022. Inner membrane complex proteomics reveals a palmitoylation regulation critical for intraerythrocytic development of malaria parasite. eLife 11:e77447.

22. Brusini L, Dos Santos Pacheco N, Tromer EC, Soldati-Favre D, Brochet M. 2022. Composition and organization of kinetochores show plasticity in apicomplexan chromosome segregation. J Cell Biol 221:e202111084.

23. Dos Santos Pacheco N, Brusini L, Haase R, Tosetti N, Maco B, Brochet M, Vadas O, Soldati-Favre D. 2022. Conoid extrusion regulates glideosome assembly to control motility and invasion in Apicomplexa. Nat Microbiol 7:1777–1790.

24. Zeeshan M, Rea E, Abel S, Vukušić K, Markus R, Brady D, Eze A, Rashpa R, Balestra AC, Bottrill AR, Brochet M, Guttery DS, Tolić IM, Holder AA, Le Roch KG, Tromer EC, Tewari R. 2023. Plasmodium ARK2 and EB1 drive unconventional spindle dynamics, during chromosome segregation in sexual transmission stages. Nat Commun 14:5652.

25. Atchou K, Berger BM, Heussler V, Ochsenreiter T. 2023. Pre-gelation staining expansion microscopy for visualisation of the Plasmodium liver stage. Journal of Cell Science 136:jcs261377.

26. Loubens M, Marinach C, Paquereau C-E, Hamada S, Hoareau-Coudert B, Akbar D, Franetich J-F, Silvie O. 2023. The claudin-like apicomplexan microneme protein is required for gliding motility and infectivity of Plasmodium sporozoites. PLOS Pathogens 19:e1011261.

27. Dubey JP. 2016. Toxoplasmosis of Animals and Humans. CRC Press.

28. Dubey JP, Lindsay DS, Speer CA. 1998. Structures of Toxoplasma gondii tachyzoites, bradyzoites, and sporozoites and biology and development of tissue cysts. Clin Microbiol Rev 11:267–299.

29. Montoya J, Liesenfeld O. 2004. Toxoplasmosis. The Lancet 363:1965–1976.

30. Tomita T, Bzik DJ, Ma YF, Fox BA, Markillie LM, Taylor RC, Kim K, Weiss LM. 2013. The Toxoplasma gondii cyst wall protein CST1 is critical for cyst wall integrity and promotes bradyzoite persistence. PLoS Pathog 9:e1003823.

31. Weiss LM, Laplace D, Takvorian PM, Tanowitz HB, Cali A, Wittner M. 1995. A cell culture system for study of the development of Toxoplasma gondii bradyzoites. J Eukaryot Microbiol 42:150–157.

32. Ferreira da Silva M da F, Barbosa HS, Groß U, Lüder CGK. 2008. Stress-related and spontaneous stage differentiation of Toxoplasma gondii. Molecular BioSystems 4:824.

33. Mouveaux T, Roger E, Gueye A, Eysert F, Huot L, Grenier-Boley B, Lambert J-C, Gissot M. 2021. Primary brain cell infection by Toxoplasma gondii reveals the extent and dynamics of parasite differentiation and its impact on neuron biology. Open Biol 11:210053.

34. Christiansen C, Maus D, Hoppenz E, Murillo-León M, Hoffmann T, Scholz J, Melerowicz F, Steinfeldt T, Seeber F, Blume M. 2022. In vitro maturation of Toxoplasma gondii bradyzoites in human myotubes and their metabolomic characterization. Nat Commun 13:1168.

35. Buchholz KR, Fritz HM, Chen X, Durbin-Johnson B, Rocke DM, Ferguson DJ, Conrad PA, Boothroyd JC. 2011. Identification of Tissue Cyst Wall Components by Transcriptome Analysis of In Vivo and In Vitro Toxoplasma gondii Bradyzoites. Eukaryotic Cell 10:1637–1647.

36. Tomita T, Sugi T, Yakubu R, Tu V, Ma Y, Weiss LM. 2017. Making Home Sweet and Sturdy: Toxoplasma gondii ppGalNAc-Ts Glycosylate in Hierarchical Order and Confer Cyst Wall Rigidity. mBio 8.

37. Zhang YW, Halonen SK, Ma YF, Wittner M, Weiss LM. 2001. Initial Characterization of CST1, a Toxoplasma gondii Cyst Wall Glycoprotein. Infect Immun 69:501–507.

38. Guevara RB, Fox BA, Falla A, Bzik DJ. 2019. Toxoplasma gondii Intravacuolar-Network-Associated Dense Granule Proteins Regulate Maturation of the Cyst Matrix and Cyst Wall. mSphere 4:e00487-19.

39. Griffith MB, Pearce CS, Heaslip AT. 2022. Dense granule biogenesis, secretion, and function in Toxoplasma gondii. J Eukaryot Microbiol 69:e12904.

40. Caffaro CE, Boothroyd JC. 2011. Evidence for Host Cells as the Major Contributor of Lipids in the Intravacuolar Network of Toxoplasma-Infected Cells. Eukaryotic Cell 10:1095–1099.

41. Nolan SJ, Romano JD, Coppens I. 2017. Host lipid droplets: An important source of lipids salvaged by the intracellular parasite Toxoplasma gondii. PLOS Pathogens 13:e1006362.

42. Dou Z, McGovern OL, Di Cristina M, Carruthers VB. 2014. Toxoplasma gondii Ingests and Digests Host Cytosolic Proteins. mBio 5:10.1128/mbio.01188-14.

43. Mercier C, Dubremetz J-F, Rauscher B, Lecordier L, Sibley LD, Cesbron-Delauw M-F. 2002. Biogenesis of Nanotubular Network in ToxoplasmaParasitophorous Vacuole Induced by Parasite Proteins. MBoC 13:2397–2409.

44. Mercier C, Howe DK, Mordue D, Lingnau M, Sibley LD. 1998. Targeted Disruption of the GRA2 Locus inToxoplasma gondii Decreases Acute Virulence in Mice. Infection and Immunity 66:4176–4182.

45. Fox BA, Guevara RB, Rommereim LM, Falla A, Bellini V, Pètre G, Rak C, Cantillana V, Dubremetz J-F, Cesbron-Delauw M-F, Taylor GA, Mercier C, Bzik DJ. 2019. Toxoplasma gondii Parasitophorous Vacuole Membrane-Associated Dense Granule Proteins Orchestrate Chronic Infection and GRA12 Underpins Resistance to Host Gamma Interferon. mBio 10:e00589-19.

46. Ferguson DJP. 2004. Use of molecular and ultrastructural markers to evaluate stage conversion of Toxoplasma gondii in both the intermediate and definitive host. International Journal for Parasitology 34:347–360.

47. Malaker SA, Pedram K, Ferracane MJ, Bensing BA, Krishnan V, Pett C, Yu J, Woods EC, Kramer JR, Westerlind U, Dorigo O, Bertozzi CR. 2019. The mucin-selective protease StcE enables molecular and functional analysis of human cancer-associated mucins. Proceedings of the National Academy of Sciences 116:7278–7287.

48. Waldman BS, Schwarz D, Wadsworth MH, Saeij JP, Shalek AK, Lourido S. 2020. Identification of a Master Regulator of Differentiation in *Toxoplasma*. Cell 180:359-372.e16.

49. Gambarotto D, Hamel V, Guichard P. 2021. Ultrastructure expansion microscopy (U-ExM). Methods Cell Biol 161:57–81.

50. Pedram K, Shon DJ, Tender GS, Mantuano NR, Northey JJ, Metcalf KJ, Wisnovsky SP, Riley NM, Forcina GC, Malaker SA, Kuo A, George BM, Miller CL, Casey KM, Vilches-Moure JG, Ferracane MJ, Weaver VM, Läubli H, Bertozzi CR. 2023. Design of a mucin-selective protease for targeted degradation of cancer-associated mucins. Nat Biotechnol https://doi.org/10.1038/s41587-023-01840-6.

51. Damstra HG, Mohar B, Eddison M, Akhmanova A, Kapitein LC, Tillberg PW. 2022. Visualizing cellular and tissue ultrastructure using Ten-fold Robust Expansion Microscopy (TREx). eLife 11:e73775.

52. Gaskins E, Gilk S, DeVore N, Mann T, Ward G, Beckers C. 2004. Identification of the membrane receptor of a class XIV myosin in Toxoplasma gondii. J Cell Biol 165:383–393.

53. Tosetti N, Dos Santos Pacheco N, Bertiaux E, Maco B, Bournonville L, Hamel V, Guichard P, Soldati-Favre D. 2020. Essential function of the alveolin network in the subpellicular microtubules and conoid assembly in Toxoplasma gondii. Elife 9:e56635.

54. Craver MPJ, Rooney PJ, Knoll LJ. 2010. Isolation of Toxoplasma gondii development mutants identifies a potential proteophosphogylcan that enhances cyst wall formation. Mol Biochem Parasitol 169:120–123.

55. Tomita T, Ma Y, Weiss L. 2018. Characterization of a SRS13: a new cyst wall mucin-like domain containing protein. Parasitol Res 117:2457–2466.

56. Tu V, Mayoral J, Sugi T, Tomita T, Han B, Ma YF, Weiss LM. 2019. Enrichment and Proteomic Characterization of the Cyst Wall from In Vitro Toxoplasma gondii Cysts. mBio 10:e00469-19.

57. Tu V, Tomita T, Sugi T, Mayoral J, Han B, Yakubu RR, Williams T, Horta A, Ma Y, Weiss LM. 2020. The Toxoplasma gondii Cyst Wall Interactome. mBio 11:e02699-19.

58. Sibley LD, Niesman IR, Parmley SF, Cesbron-Delauw MF. 1995. Regulated secretion of multi-lamellar vesicles leads to formation of a tubulo-vesicular network in host-cell vacuoles occupied by Toxoplasma gondii. Journal of Cell Science 108:1669–1677.

59. Nadipuram SM, Thind AC, Rayatpisheh S, Wohlschlegel JA, Bradley PJ. 2020. Proximity biotinylation reveals novel secreted dense granule proteins of Toxoplasma gondii bradyzoites. PLOS ONE 15:e0232552.

60. Cheng Z, Stefani C, Skillman T, Klimas A, Lee A, DiBernardo EF, Brown KM, Milman T, Wang Y, Gallagher BR, Lagree K, Jena BP, Pulido JS, Filler SG, Mitchell AP, Hiller NL, Lacy-Hulbert A, Zhao Y. 2023. MicroMagnify: A Multiplexed Expansion Microscopy Method for Pathogens and Infected Tissues. Advanced Science 10:2302249.

Supplementary data

Supplementary movie 1

The GRA2 granules in the expanded cyst span through the CST1-positive layer.

ME49Δku80ΔhxgprtME49 bradyzoite cysts grown in HFFs for 7 days, probed with antibodies against GRA2 (green) and CST1 (magenta), and expanded using UExM+StcE protocol as in Figure 4. The video shows the z axis of azoomed-in part of the three expanded cyst walls facing the host cell environment (left hand side). The arrows indicate the direction of movement along z axis. The “up” arrow indicate the movement away from the glass coverslip towards the top of the cyst, and the “down” arrow vice versa. The video demonstrates GRA2 puncta “spanning” in or around the CST1-positive layer of the cyst wall.